

Supporting information

Fluorescence and electrochemical integrated dual-signal sensor for detection of iron ion in water based on ITO substrate

Zhenyu Bai^a, Ping Li^a, Hao Fu^a, Peicai Chen^a, Xiaoyang Feng^a, Xueping Hu^{a,*}, Xingliang Song^{a,*} and Lingxin Chen^{b, c, d}

^a School of Chemistry and Chemical Engineering, Linyi University, Linyi, 276005, P.R. China

^b CAS Key Laboratory of Coastal Environmental Processes and Ecological Remediation, Research Center for Coastal Environmental Engineering and Technology, Yantai Institute of Coastal Zone Research, Chinese Academy of Sciences, Yantai 264003, China

^c School of Pharmacy, Binzhou Medical University, Yantai, 264003, China

^d School of Environmental & Municipal Engineering, Qingdao University of Technology, Qingdao 266033, China

*Corresponding author.

Xueping Hu, E-mail: xuephu@yeah.net; Xingliang Song, E-mail: xlssong@yeah.net

Contents

SI.1 Chemicals and Instruments.....	2
SI.2 Quantum yield calculation	2
SI.3 Characterization section	2
SI.4 The UV-vis spectra	3
SI.5 Decay curves and Zeta potential.....	3
SI.6 Optimization of Fe ³⁺ detection.....	5
SI.7 Interference experiment.....	5
SI.8 Detection of actual water sample.....	6
SI.9 Tables	6
References	7

SI.1 Chemicals and Instruments

All reagents and analytical were of analytical grades. Iron (III) chloride hexahydrate, and Fluorescein5(6)-isothiocyanate (FITC) were purchased from Shanghai Macklin Biochemical Co., Ltd (Shanghai, China). 7-Hydroxy-4-methylcoumarin (4-MU) was obtained from J&K Scientific Co., Ltd. (Beijing, China). Methanol, acetonitrile, dimethylformamide (DMF), H₂O₂, and Chitosan were obtained from Sinopharm Chemical Reagent Co., Ltd (Shanghai, China). Sodium hydroxide and ethanol were obtained from Tianjin Hengxing Chemical Preparation Co., Ltd (Tianjin, China). Standard samples of environmental iron were purchased from Beijing Manhage Bio-Tech Co., Ltd. (Beijing, China). ITO electrode was designed by ourselves and customized by South China Science & Technology Co., Ltd.

The morphology and SEM elemental mapping of Chi-FITC-4MU was characterized by Hitachi SU8010 scanning electron microscopy (SEM, Guangzhou, China). Zeta potential was characterized on Nano ZS90 (Shanghai, China). FT-IR absorption was recorded on FTIR-650 purchased by GangDong Scientific and Technical Co., Ltd (GangDong, China). UV-vis absorption spectra were obtained by TU-1901 spectrophotometer (Beijing, China). Fluorescence emission was obtained by Cary Eclipse (Beijing, China). All electrochemical detection were carried out on CHI660E (Shanghai, China).

SI.2 Quantum yield calculation

By taking rhodamine B in ethanol (QY = 0.89) as reference, quantum yield of the FITC and as-synthesized Chi-FITC-4MU was estimated. The quantum yield was calculated by using the following equation^{1,2}.

$$\Phi_x = \frac{I_x}{\Phi_r} \cdot \frac{A_x}{A_r} \cdot \frac{\eta_x^2}{\eta_r^2}$$

Where the subscripts “x” and “r” are assigned for Chi-FITC-4MU and rhodamine B respectively. “Φ” is fluorescent quantum yield. “I” designates the integrated fluorescence emission intensity, “A” denotes the absorbance measured at 340 nm and “η” is the refractive index of the solution in distilled water.

SI.3 Characterization section

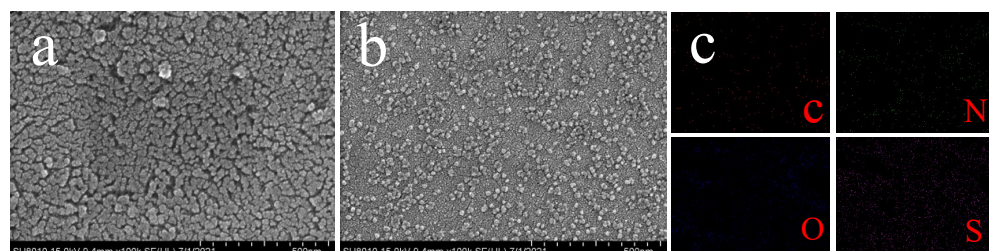


Fig. S1. SEM images of (a) bare Chi, (b) Chi-FITC-4MU, (c) SEM elemental mapping showing the presence of C, O, N, S.

SI.4 The UV-vis spectra

In general, the absorption or reflection intensity of substance molecules to monochromatic radiation in the ultraviolet-visible band range (150 – 800 nm) is different, so qualitative analysis and molecular structure analysis of various chemical substances can be carried out according to the intensity of absorption and reflection. Therefore, Fe^{3+} , Chi-FITC-4MU and Chi-FITC-4MU- Fe^{3+} were characterized by the ultraviolet spectrum, as shown in Fig. S2. It can be clearly observed that Fe^{3+} had a very flat peak shape at 320 nm, while Chi-FITC-4MU- Fe^{3+} had an ultraviolet peak bulge at the same position, and compared with Chi-FITC-4MU, the UV-vis absorption peaks of hybrid materials Chi-FITC-4MU- Fe^{3+} peaks down and emerged a blue shift at 320 nm, demonstrating that Fe^{3+} binds to Chi-FITC-4MU to generate the complex.

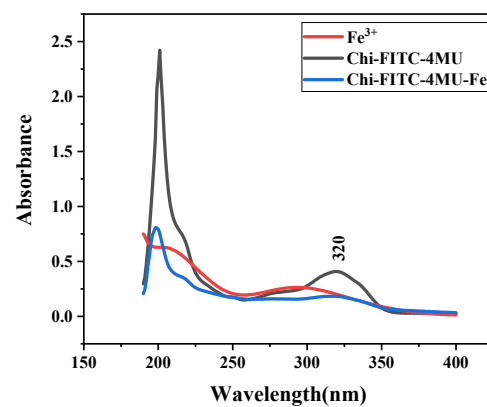


Fig. S2. UV-vis absorption spectrum of Chi-FITC-4MU (blank line), 0.1 mM Fe^{3+} (red line) and Chi-FITC-4MU- Fe^{3+} (blue line).

SI.5 Decay curves and Zeta potential

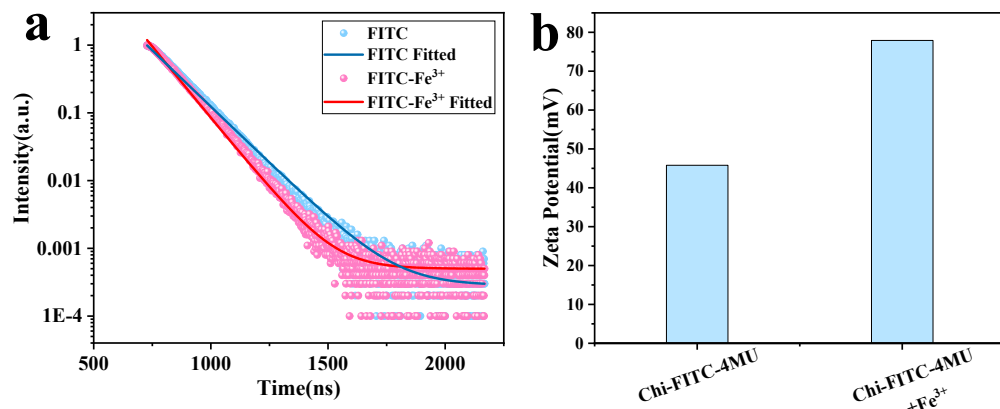


Fig. S3. (a) Decay curves of FITC and FITC- Fe^{3+} . (b) Zeta potentials of Chi-FITC-4MU and Chi-FITC-4MU- Fe^{3+} .

SI.6 Optimization of Fe^{3+} detection

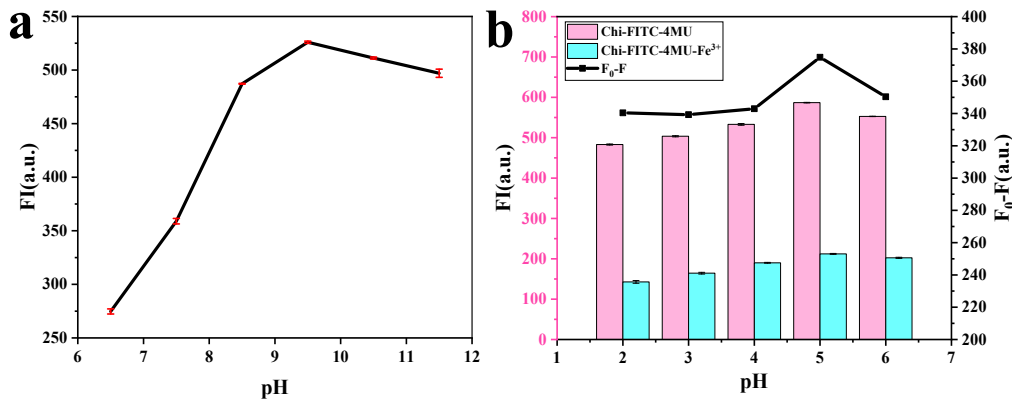


Fig. S4. The effect of pH-I (a), and pH-II (b) on the fluorescence procedure. Experimental conditions are the following: pH-I, 9.5; pH-II, 5.0.

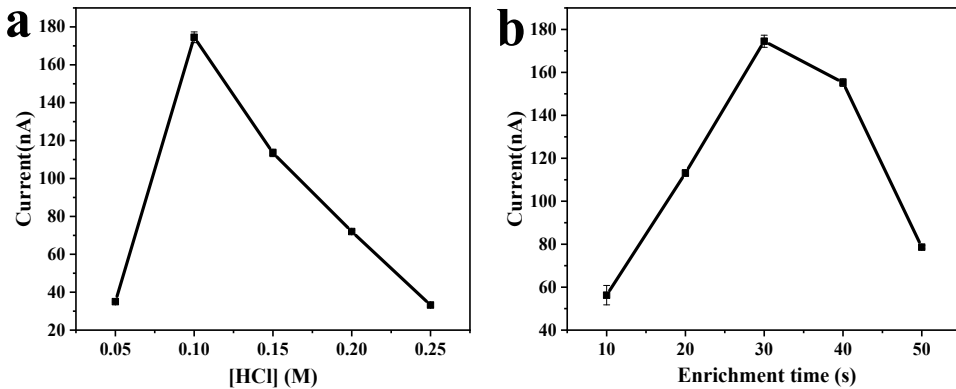


Fig. S5. The effect of HCl electrolyte solution concentration (a), enrichment time (b) on the electrochemical detection procedure.

SI.7 Interference experiment

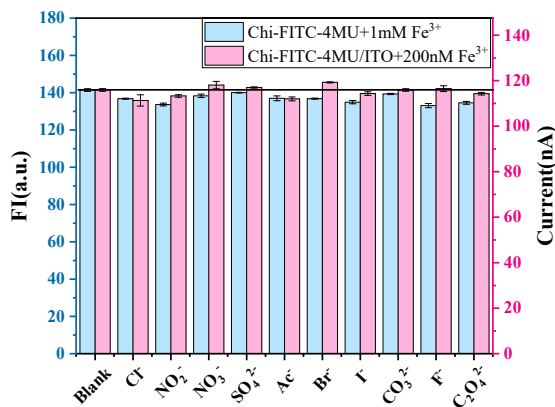


Fig. S6. Electrochemical and fluorescence response of Chi-FITC-4MU/ITO towards various interfering anions.

SI.8 Detection of actual water sample

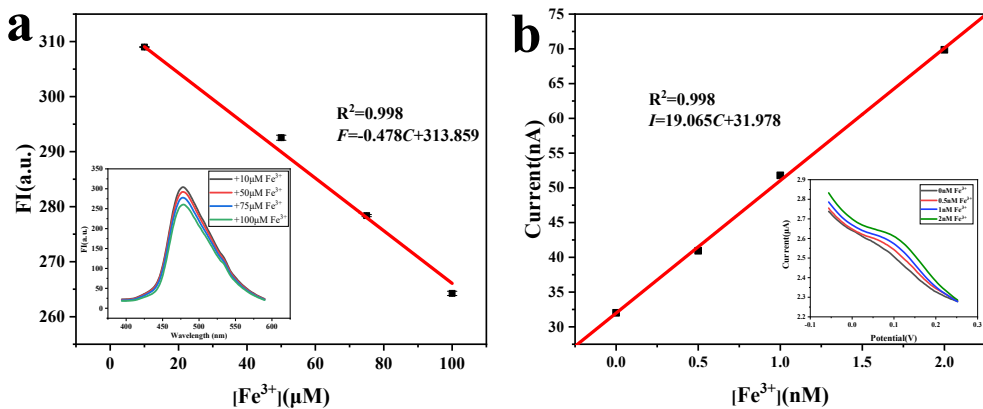


Fig. S7. Corresponding curve for the determination of Fe^{3+} in standard samples of environmental iron (a) by the standard addition method. The inset shows the fluorescence spectra. Corresponding curve for the determination of Fe^{3+} in standard samples of environmental iron (b) by the standard addition method. The inset shows the voltammograms.

SI.9 Tables

Table S1. Comparison of our sensor performance with various other reported fluorescent materials.

Materials ^a	LOD (μM)	Linear range (μM)	Response Time (min)	Ref
NCDs	0.31	3–60	1	3
Phe-CDs	0.72	5–500	30	4
P, Cl-CDs	0.06	0.1–8	—	5
F-CDs	0.01	1–100	10	6
TTA	0.19	0.0–10	1	7
CPs	2.75	0–60	30	8
Cd-CP	3.24	0–25	30	9
R6G/CDs	0.73	0–50	5	10
AuEHs	0.0014	0.099–137	5.7	11
P(AM-co-MBA-co-RhBUEA)	0.088	0–55	20	12
Chi-FITC-4MU	0.12	0.1–100	0.5	This work

^a NCDs: N-doped carbon dots; Phe-CDs: the carbon dots made from phenylalanine; P, Cl-CDs: phosphorus and chlorine co-doped carbon dots; F-CDs: F-doped carbon dots; TTA: terthiophene-derived colorimetric and fluorescent dual-channel sensor; CPs: coordination polymers using 2-deoxy-D-ribose derivatives as ligands; Cd-CP: Cd-based coordination polymer; R6G/CDs: rhodamine 6G functionalized carbon dots; AuEHs: H^+ -triggered self-assembled gold nanoclusters; P (AM-co-MBA-co-RhBUEA): rhodamine-functionalized polyacrylamide hydrogel.

Table S2. Comparison of our sensor performance with various other reported electrochemical detection.

Materials ^a	Technique ^b	Electrode ^c	LOD (nM)	Linear rang (nM)	Ref
Co-based CPs	i-t	CPE	5840	10 ⁴ –10 ⁶	13
Co-MOF	CV	GCE	100	100–1200	14
PEDOT-DFA nanowires	CV	DFA	10	10–10 ⁵	15
TCPP NS-GO	ECL	GCE	0.01	1–100	16
4a-i	CV	GCE	52	100–400	17
DHN	CSV	HMDE	0.005	—	18
nano-TiC	SWV	GCE	7.2	70–7×10 ⁴	19
4	CV	GCE	137	—	20
CPE-SB	DPV	CPE	50	100–10 ⁷	21
Chi-FITC-4MU	SWV	ITO	0.0182	0.1–500	This work

^a Co-based CPs: cobalt-Based coordination polymer crystalline; Co-MOF: co based metal organic anion framework; PEDOT-DFA nanowires: potentiostatically deposited from a solution containing both EDOT and DFA using lithographically patterned nanowire electrodeposition; TCPP NS-GO: luminophore porphyrin nanosphere–graphene oxide composite; 4a-i: Benzo [4,5] thiazolo [3, 2-a] pyrimidine-3-carboxylate derivatives; DHN: Fe/2, 3-dihydroxynaphthalene; nano-TiC: titanium carbide nanoparticles; 4: fluorescein-based chemosensor containing a ferrocene backbone has been designed; CPE-SB: the carbon paste electrode incorporating Schiff-base ionophore 1,10-((ethane-1,2-diylbis(oxy))bis (2,1-phenylene)) bis(N-p-tolylmethanimine).

^b i-t: amperometric i-t cure; ECL: electrochemiluminescence; CSV: cathodic stripping voltammetry; DPV: differential pulse voltammograms.

^c CPE: carbon paste electrode; DFA: deferoxamine.

References

- 1 N. Chaudhary, P. K. Gupta, S. Eremin and P. R. Solanki, Journal of Environmental Chem. Eng., 2020, **8**, 2213–3437.
- 2 Y. D. Hang, J. Wang, T. Jiang, N. N. Lu and J. L. Hua, Anal. Chem., 2016, **88**, 1696–1703.
- 3 B. Rajkumar, D. Ramakrishna, R. G. Bhagavanth, K. S. Fedlu, A. Madhusudhan, S. H. Lee and G. Veerabhadram, Microchim. Acta., 2020, **187**, 30–39.
- 4 Z. F. Pu, Q. Lin Wen, Y. J. Yang, X. M. Cui, J. Ling, P. Liu and Q. E. Cao, Spectrochimi, Spectrochim Acta A., 2020, **229**, 117944.
- 5 W. Wang, J. Peng and F. Li, Microchim. Acta., 2019, **186**, 32–39.
- 6 D. Hong, X. Y. Deng, J. M. Liang, J. Y. Li, T. Yi and K. J. Tan, Microchem J., 2019, **151**, 104217.
- 7 J. Wang, T. Wei, F. Ma, T. Li and Q. Niu, J. Photoch. Photobio. A., 2019, **383**, 111982.
- 8 T. S. He, Y. L. Lan, Z. Y. Li, L. N. Zhu and X. Z. Li, Cryst Growth Des., 2021, **21**, 2233–2242.
- 9 Y. Yu, Y. Wang, H. Yan, J. Lu, H. Liu, Y. Li, S. Wang, D. Li, J. Dou, L. Yang and Z. Zhou, Inorg. Chem., 2020, **59**, 3828–3837.
- 10 M. Deng, S. Wang and C. Liang, RSC Adv., 2016, **6**, 26936–26940.
- 11 W. Y. Li, X. P. Wen, H. M. Zhao, W. J. Yan, J. F. Trant, and Y. Q. Li, ACS Appl. Nano Mater., 2020, **3(12)**, 11838–11849.
- 12 X. Y. Liu, Z. Chen, R. S. Gao, C. Y. Kan and J. H. Xu, Sensor Actuat B-Chem., 2021, **340**, 129958.

- 13 Y. Wang, J. X. Ma, Y. Zhang, N. Xu and X. L. Wang, Cryst Growth Des., 2021, **21**, 4390-4397.
- 14 L. Y. Pang, P. Wang, J. J. Gao, Y. Wen and H. Liu, J. Electroanal Chem., 2019, **836**, 85-93.
- 15 L. R. Kindra, C. J. Eggers, A. T. Liu, K. Mendoza, J. Mendoza, A. R. Klein Myers and R. M. Penner, Anal. Chem., 2015, **87**, 11492-500.
- 16 L. Li, X. Ning, Y. Qian, G. Pu, Y. Wang, X. Zhang, H. Wang, J. Chen, D. Shan and X. Lu, Sensor Actuat B-Chem., 2018, **257**, 331-339.
- 17 S. Seenan and S. Kulathu Iyer, J. Org. Chem., 2020, **85**, 1871-1881.
- 18 S. Caprara, L. M. Laglera and D. Monticelli, Anal. Chem., 2015, **87**, 6357-63.
- 19 M. Y. Lin, D. Pan, X. P. Hu, H. Han and F. Li, Sensor Actuat B-Chem., 2015, **219**, 164-170.
- 20 S. R. Bhatta, A. Pal, U. K. Sarangi and A. Thakur, Inorganica Chimica Acta, 2019, **498**, 119097.
- 21 S. Kaur, B. A. Shiekh, D. Kaur and I. Kaur, Journal of Molecular Liquids, 2021, **333**, 115954.